

Hybrid Density Functional Study of Structural and Electronic Properties of Functionalized $\text{Ti}_{n+1}\text{X}_n$ ($\text{X} = \text{C}, \text{N}$) monolayers

Yu Xie^{1,*} and P. R. C. Kent^{1,2}

¹*Center for Nanophase Materials Sciences,
Oak Ridge National Laboratory, Oak Ridge, Tennessee 37831, USA*

²*Computer Science and Mathematics Division,
Oak Ridge National Laboratory, Oak Ridge, Tennessee 37831, USA*

(Dated: November 27, 2024)

Abstract

Density functional theory simulations with conventional (PBE) and hybrid (HSE06) functionals were performed to investigate the structural and electronic properties of MXene monolayers, $\text{Ti}_{n+1}\text{C}_n$ and $\text{Ti}_{n+1}\text{N}_n$ ($n = 1-9$) with surfaces terminated by O, F, H, and OH groups. We find that PBE and HSE06 give similar results. Without functional groups, MXenes have magnetically ordered ground states. All the studied materials are metallic except for Ti_2CO_2 , which we predict to be semiconducting. The calculated density of states at the Fermi level of the thicker MXenes ($n \geq 5$) is much higher than for thin MXenes, indicating that properties such as electronic conductivity and surface chemistry will be different. In general, the carbides and nitrides behave differently with the same functional groups.

PACS numbers: 71.20.-b, 71.20.Be, 73.20.-r

I. INTRODUCTION

The study of two-dimensional (2D) materials is a topic of current interest, not only for their unique properties¹⁻³ compared with their three-dimensional (3D) counterparts, but also for their important applications to industry and engineering⁴⁻⁷. Over the years, despite many experimental efforts on 2D materials, only a few classes of freestanding single-layer 2D materials have been successfully synthesized. Among them, the very first and most fascinating one is graphene¹ which is prepared from exfoliated graphite. Other graphene-like materials, such as hexagonal BN and dichalcogenides, are synthesized by exfoliation of their 3D-layered precursors.⁸⁻¹⁰ Normally, these compounds are considered as van der Waals solids due to the weak interaction between layers, making them able to be exfoliated. Alternatively, the synthesis of freestanding 2D monolayers from 3D-layered solids with strong interlayer bonds is more difficult.

Very recently, a new family of 2D materials was prepared by the exfoliation of the layered ternary transition metal carbides, which are known as MAX phase^{11,12}. The latter is a large family of layered solids, including ternary transition metal carbides, nitrides, and carbonitrides, with more than 70 members. The MAX phases usually possess unique properties, such as remarkable machinability, high damage tolerance, excellent oxidation resistance, and high electrical and thermal conductivity, with various industrial applications.¹³⁻¹⁵ These solids have a general formula of $M_{n+1}AX_n$ ($n = 1, 2, 3, \dots$), where “M” is an early transition metal, “A” represents the main group elements (mostly group IIIA and IVA), and “X” denotes C and/or N. MAX phases adopt hexagonal structures (space group $P63/mmc$), and their structures can be viewed as inter-growth structures consisting of hexagonal $M_{n+1}X_n$ layers and planar A atomic sheets with alternative stacking along the c direction. The crystal structure of M_3AX_2 is shown in Fig. 1(a) as an example. In general, the MAX phases are quite stable. However, compared to the strong M–X intralayer bonds, the interatomic A–A bonds and interlayer M–A bonds are weaker, making A atomic layers chemically more reactive. In turn, taking Ti_3AlC_2 as an example, the Al layers can be extracted from the solid Ti_3AlC_2 by hydrofluoric acid treatment and sonication, resulting in graphene-like Ti_3C_2 nanosheets, so-called “MXene”.¹⁶ Depending on the synthesis conditions, the surfaces of Ti_3C_2 monolayers are chemically terminated with oxygen-containing and/or fluoride groups. Following the same procedure, other MXenes, including Ti_2C , Ta_4C_3 , Ti_3CN ,

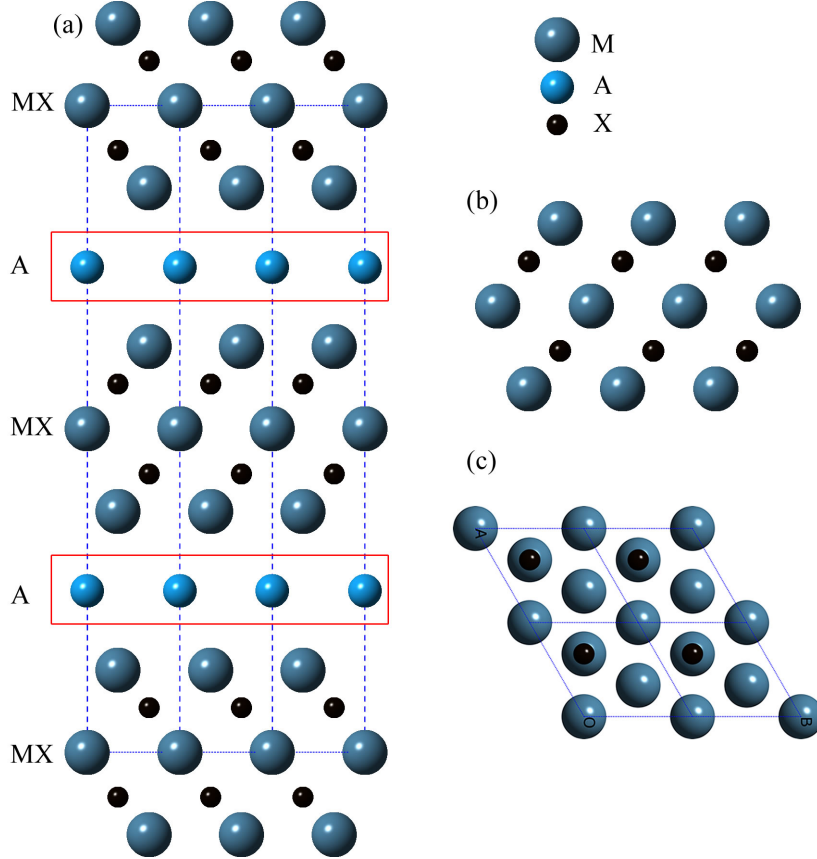


FIG. 1. (color online) (a) Crystal structure of layered M_3AX_2 solid phase. The M_3X_2 and A layer are stacked in a zigzag formation. (b) and (c) Side and top views of M_3X_2 monolayer.

$(Ti_{0.5}Nb_{0.5})_2C$, and $(Ti_{0.5}Cr_{0.5})_2C$, have been prepared by exfoliation of the corresponding carbides and carbonitrides.¹⁷ Notably, due to the large number of MAX family, it is predictable that more MXenes will be synthesized by exfoliation of their corresponding MAX phases.

Several studies^{16–26} have been conducted to understand the properties of these newly discovered graphene-like MXenes. It has been shown that these materials are good electrical conductors^{16–18} and have high elastic moduli¹⁹. The intercalation of Li ion and organic molecules into Ti_2C ^{20,21}, Ti_3C_2 ^{22,23}, Ti_3CN ²³, and $TiNbC$ ²³ sheets suggests they are promising candidates for Li-ion battery anodes and hybrid electrochemical capacitors. And with proper termination groups, the functionalized MXenes could become semiconductors with large Seebeck coefficients as potential thermoelectric materials.²⁴ However, up to now these studies are mainly focused on the M_2X and M_3X_2 type of MXenes, there are no reports on the properties of exfoliated carbides or nitrides with other n .

In this work, we investigate systematically the evolution of structural and electronic properties of graphene-like titanium carbide and nitride MXenes ($\text{Ti}_{n+1}\text{C}_n$ and $\text{Ti}_{n+1}\text{N}_n$, $n = 1-9$) with different functional groups (F, O, H, and OH) using conventional and hybrid density functional calculations. We show that all the studied materials are metals except for Ti_2CO_2 . With the same surface termination, carbides and nitrides exhibit different electronic properties. The density of states (DOS) at the Fermi level increases in both carbides and nitrides with distinct trends, as n increases. Moreover, the calculations suggest that the “pure” carbide and nitride monolayers are magnetic. After functionalization, magnetism is removed.

II. COMPUTATIONAL DETAILS

The first principle calculations are carried out using density functional theory (DFT) as implemented in the Vienna ab initio simulation package (VASP)²⁷. The all-electron projected argument wave (PAW) method²⁸ is used to describe the ion–electron interaction, with $1s^1$, $2s^22p^2$, $2s^22p^3$, $2s^22p^4$, $2s^22p^5$, $3s^23p^1$, and $3d^24s^2$ treated as valence electrons for H, C, N, O, F, Al, and Ti, respectively. For Ti, PAW configurations including $3s$ and/or $3p$ electrons in the valence give the similar results. For the exchange–correlation energy, we use both the Perdue–Burke–Ernzerhof (PBE) version of generalized gradient approximation (GGA)²⁹ and the Heyd–Scuseria–Ernzerhof (HSE06)^{30–32} hybrid functional. The latter can be described through the following equation:

$$E_{xc}^{HSE} = \frac{1}{4}E_x^{HF,SR}(\mu) + \frac{3}{4}E_x^{PBE,SR}(\mu) + E_x^{PBE,LR}(\mu) + E_c^{PBE}. \quad (1)$$

The PBE exchange term is split into a short range (sr) and a long-range (lr) part. Then, 25% of short range part is replaced by a short range Hartree–Fock term. The correlation part of PBE is not changed. The screening parameter in HSE was fixed at a value of 0.2 \AA^{-1} . This functional obtains improved formation energies and more reliable band gaps than PBE,^{30,33} and is therefore better able to identify stable structures and the metallic or insulating character of the MXenes.

A plane wave cutoff energy of 580 eV is sufficient to ensure the convergency of total energies to 1 meV per primitive cell. The underlying structural optimization are performed using the conjugated gradient method, and the convergency criterion was set to 10^{-6} eV/cell

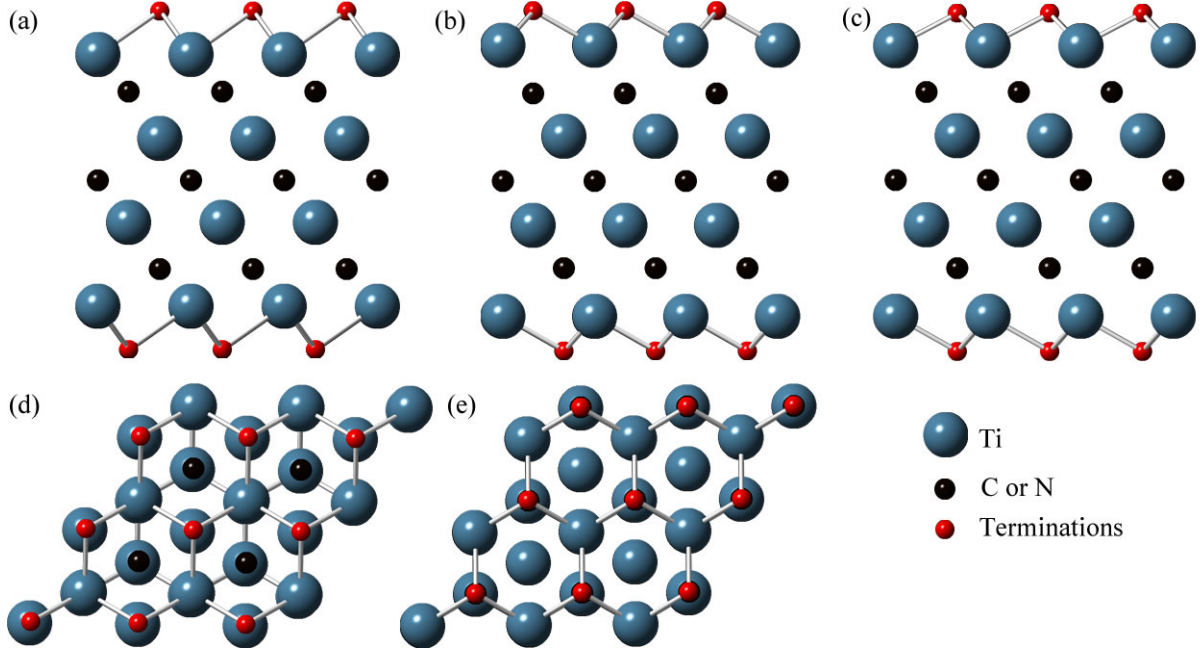


FIG. 2. (color online) Structure configurations of functionalized MXenes with different arrangements of the surface atoms: side views of (a) I-Ti₄X₃T₂, (b) II-Ti₄X₃T₂, and (c) III-Ti₄X₃T₂; (d) and (e) top views of I-Ti₄X₃T₂ and II-Ti₄X₃T₂. Since configuration III is a mixture of I and II, the top view of III is not shown.

in energy and 0.005 eV/Å in force. A loose $12 \times 12 \times 1$ Monkhorst-Pack k grid is used during the optimization. To avoid any interaction between an MXene sheet and its periodically repeated images along the c axis, a large vacuum space of 20 Å is used. After full structural optimization, a denser k grid of $42 \times 42 \times 1$ and $20 \times 20 \times 1$ is employed in the calculation of electronic properties for PBE and HSE06, respectively. The computational cost of HSE06 precludes use of the largest k -point grids.

III. STRUCTURAL MODELS

In order to examine the evolution of the electronic properties of MXenes, we have studied the structural, magnetic, and electronic properties of a series of carbides Ti_{*n*+1}C_{*n*} and nitrides Ti_{*n*+1}N_{*n*}, with n up to 9. The 2D MXenes are constructed appropriately by removing “A” atoms from their bulk MAX phases (Fig. 1(b)). It is noteworthy that, for the parent MAX phases we used, the Ti₂AlC,³⁴ Ti₃AlC₂,¹⁴ Ti₄GeC₃,³⁵ (TiNb)₅AlC₄,³⁶ Ti₇SnC₆,³⁷ Ti₂AlN,³⁴ and Ti₄AlN₃³⁸ have been synthesized experimentally. The unknown MAX phases

($\text{Ti}_{n+1}\text{AlC}_n$, $n = 5, 7-9$, and $\text{Ti}_{n+1}\text{AlN}_n$, $n = 2, 4-9$) are built up by following a generalized modular building principle proposed by Etzkorn and co-workers.¹¹ The calculated lattice parameters of all studied MAX phases are shown in Table I and compared with available experimental data^{14,34-38} and previous theoretical results^{25,39,40}. The consistency of the results in both experiment and theory make us confident for further studies. Notably, it has been reported that the surfaces of MXenes are covered with oxygen-containing groups, such as OH, and fluorine, F.¹⁶ As a consequence, the chemistry of exfoliated MXenes is expected to be closer to the functionalized MXenes than the bare material. It also could be possible to create O-termination surfaces by post-processing of OH-terminated systems.²⁴

TABLE I. Calculated PBE equilibrium lattice parameter (a , c , and c/a) for MAX phases in comparison with available experimental data and previous theoretical results.

$\text{Ti}_{n+1}\text{AC}_n$		a (Å)	c (Å)	c/a	$\text{Ti}_{n+1}\text{AN}_n$		a (Å)	c (Å)	c/a
Ti_2AlC	PBE	3.0687	13.7266	4.47	Ti_2AlN	PBE	2.9965	13.6400	4.55
	Theo. ^a	3.0694	13.7311	4.47		Theo. ^a	2.9965	13.6360	4.55
	Exp. ^b	3.065	13.71	4.48		Exp. ^b	2.986	13.60	4.55
Ti_3AlC_2	PBE	3.0816	18.6379	6.05	Ti_3AlN_2	PBE	3.0036	18.5007	6.16
	Theo. ^a	3.0824	18.6522	6.05		Theo. ^a	3.0065	18.4780	6.15
	Exp. ^c	3.075	18.58	6.04					
Ti_4GeC_3	PBE	3.0868	22.8515	7.40	Ti_4AlN_3	PBE	2.9975	23.4803	7.83
	Theo. ^d	3.088	22.852	7.40		Theo. ^a	2.9975	23.4828	7.83
	Exp. ^e	3.088	22.852	7.40		Exp. ^f	2.9905	23.380	7.82
Ti_5AlC_4	PBE	3.0791	28.7440	9.34	Ti_5AlN_4	PBE	2.9928	28.6249	9.56
	Theo. ^g	3.074	28.76	9.35		Theo. ^h	3.00	28.44	9.48
$(\text{TiNb})_5\text{AlC}_4$	Exp. ^g	3.100	28.89	9.32					
Ti_6AlC_5	PBE	3.0841	33.5105	10.86	Ti_6AlN_5	PBE	3.0011	33.3420	11.11
Ti_7SnC_6	PBE	3.1604	40.5154	12.82	Ti_7AlN_6	PBE	3.0017	38.2657	12.75
	Exp. ⁱ	3.200	41.000	12.81					
Ti_8AlC_7	PBE	3.0817	43.4258	14.09	Ti_8AlN_7	PBE	3.0036	43.1310	14.36
Ti_9AlC_8	PBE	3.0878	48.1608	15.59	Ti_9AlN_8	PBE	3.0132	47.7686	15.85
$\text{Ti}_{10}\text{AlC}_9$	PBE	3.0885	53.1124	17.19	$\text{Ti}_{10}\text{AlN}_9$	PBE	3.0145	52.6603	17.47

^a Ref. 25, VASP-PBE.

^b Ref. 34, XRD.

^c Ref. 14, XRD.

^d Ref. 39, DFT-GGA.

^e Ref. 35, XRD.

^f Ref. 38, XRD.

^g Ref. 36, experiment, XRD/STEM; theory, CASTEP-GGA.

^h Ref. 40, FPLAPW-GGA.

ⁱ Ref. 37, XRD/DSC/HRTEM.

Moreover, the hydrogen-terminated graphene has been studied extensively due to its unique properties.⁴¹ Therefore, in our studies, we have considered that the surfaces of MXenes are fully terminated by F, O, H, and OH, with a general formula of $\text{Ti}_{n+1}\text{X}_n\text{T}_2$ ($\text{X} = \text{C}, \text{N}$, and T is the terminations). Note, for MXenes extracted from the unknown MAX phases, only the fluorine termination has been studied. According to the geometry of the MXenes, the functionalized MXenes are built up with three major possible configurations: (I) all the functional groups are located above the hollow site of three neighboring C/N atoms and pointed to the Ti atoms in the second Ti atomic layer on both sides of MXenes; (II) all the functional groups are located on top the topmost sides of C/N atoms on both sides of MXenes; (III) is a combination of (I) and (II), in which one functional group is located on top of the hollow sites of C/N atoms on one side and another one locates above the top sites of C/N atoms on other sides. These models are shown in Fig. 2. We perform full geometry optimization for each of these structures.

IV. RESULTS AND DISCUSSION

A. Structural properties

We first check the relative stability of the different structural models. The PBE total energy differences (relative to configuration I) of all configurations and terminations are listed in Table II. Configuration I usually has the lowest total energy indicating it is energetically more favorable and the configuration III normally has the highest energy. This is quite understandable, since Ti atoms are the main electron donors and the functional groups are more likely to bond with Ti atoms than C or N atoms. However, there are several exceptions. For $\text{Ti}_3\text{N}_2\text{F}_2$, configuration II has the lowest energy; whereas for $\text{Ti}_4\text{N}_3(\text{OH})_2$ and $\text{Ti}_7\text{C}_6\text{H}_2$, the configuration III is more stable. We also notice that the relative total energy differences are not very sensitive to increased layer thickness and oxygen always has the largest differences among the four functional groups for both carbides and nitrides. Moreover, the energy differences of nitrides are smaller than carbides. In general, our results are consistent with previous reports.^{22,24}

We then proceed to investigate the ground-state structural properties of the functionalized MXenes. Some of the calculated equilibrium lattice parameters a , thickness of the

TABLE II. PBE total energy differences (relative to configuration I) of functionalized $\text{Ti}_{n+1}\text{C}_n$ and $\text{Ti}_{n+1}\text{C}_n$ MXenes. The most stable configuration is highlighted in bold-typeface.

$\text{Ti}_{n+1}\text{C}_n$	$E_0 - E_0^I$ (eV)				$\text{Ti}_{n+1}\text{N}_n$	$E_0 - E_0^I$ (eV)			
	F	O	H	OH		F	O	H	OH
Ti_2C					Ti_2N				
I	0.000	0.000	0.000	0.000	I	0.000	0.000	0.000	0.000
II	0.439	1.750	0.698	0.321	II	0.398	1.175	0.533	0.296
III	0.215	0.769	0.365	0.130	III	0.427	0.546	0.299	0.266
Ti_3C_2					Ti_3N_2				
I	0.000	0.000	0.000	0.000	I	0.000			
II	0.729	1.423	0.718	0.476	II	-0.089			
III	0.371	0.712	0.349	0.240	III	-0.002			
Ti_4C_3					Ti_4N_3				
I	0.000	0.000	0.000	0.000	I	0.000	0.000	0.000	0.000
II	0.720	1.462	0.719	0.455	II	0.161	1.102	0.591	0.003
III	0.387	0.733	0.361	0.245	III	0.088	0.561	0.299	-0.003
Ti_5C_4					Ti_5N_4				
I	0.000	0.000	0.000	0.000	I	0.000			
II	0.701	1.491	0.720	0.429	II	0.051			
III	0.362	0.747	0.358	0.222	III	0.057			
Ti_6C_5					Ti_6N_5				
I	0.000				I	0.000			
II	0.720				II	0.146			
III	0.369				III	0.08			
Ti_7C_6					Ti_7N_6				
I	0.000	0.000	0.000	0.000	I	0.000			
II	0.712	1.532	0.205	0.419	II	0.093			
III	0.361	0.780	-0.154	0.213	III	0.082			
Ti_8C_7					Ti_8N_7				
I	0.000				I	0.000			
II	0.728				II	0.125			
III	0.371				III	0.072			
Ti_9C_8					Ti_9N_8				
I	0.000				I	0.000			
II	0.728				II	0.125			
III	0.368				III	0.079			
Ti_{10}C_9					Ti_{10}N_9				
I	0.000				I	0.000			
II	0.729				II	0.127			
III	0.367				III	0.074			

monolayer (vertical distance from the topmost atomic layer to bottommost atomic layer, L), and bond lengths between surface Ti atom and termination ($d_{\text{Ti-T}}$) and nearest C/N atom ($d_{\text{Ti-X}}$) with PBE and HSE06 functionals are shown and compared with other theoretical results²⁴ in Table III. Clearly, our PBE results are in good agreement with others. The HSE06 lattice parameters and bond lengths are about $0.02 \sim 0.03 \text{ \AA}$ smaller than for PBE,

TABLE III. Calculated equilibrium lattice parameter (a), thickness of the monolayer (L), and bond lengths between surface Ti atom and termination ($d_{\text{Ti-T}}$), and nearest C/N atom ($d_{\text{Ti-X}}$) of selected functionalized MXenes in comparison with previous theoretical results.

$\text{Ti}_{n+1}\text{C}_n\text{T}_2$		a (Å)	L (Å)	$d_{\text{Ti-C}}$ (Å)	$d_{\text{Ti-T}}$ (Å)	$\text{Ti}_{n+1}\text{N}_n\text{T}_2$		a (Å)	L (Å)	$d_{\text{Ti-N}}$ (Å)	$d_{\text{Ti-T}}$ (Å)
Ti_2CF_2	Theo. ^a	3.0587	4.84	2.10	2.16	Ti_2NF_2	Theo. ^a	3.0704	4.69	2.07	2.16
	PBE	3.0583	4.80	2.10	2.16		PBE	3.0642	4.63	2.07	2.16
	HSE	3.0312	4.72	2.08	2.14		HSE	3.0460	4.55	2.05	2.14
Ti_2CO_2	Theo. ^a	3.0349	4.47	2.19	1.98	Ti_2NO_2	Theo. ^a	3.0191	4.28	2.17	1.93
	PBE	3.0329	4.45	2.19	1.98		PBE	3.0030	4.35	2.15	1.98
	HSE	3.0093	4.40	2.17	1.96		HSE	2.9743	4.29	2.13	1.86
$\text{Ti}_2\text{C}(\text{OH})_2$	Theo. ^a	3.0715	6.75	2.11	2.18	$\text{Ti}_2\text{N}(\text{OH})_2$	Theo. ^a	3.0635	6.68	2.08	2.17
	PBE	3.0712	6.79	2.12	2.18		PBE	3.0635	6.66	2.08	2.17
	HSE	3.0464	6.71	2.09	2.17		HSE	3.0447	6.56	2.06	2.16
Ti_2CH_2	PBE	3.0357	4.28	2.10	2.01	Ti_2NH_2	PBE	2.9882	4.20	2.07	2.00
	HSE	3.0094	4.24	2.08	1.99		HSE	3.0127	4.11	2.04	2.00
$\text{Ti}_3\text{C}_2\text{F}_2$	Theo. ^a	3.0792	7.23	2.08	2.17	$\text{Ti}_3\text{N}_2\text{F}_2$					
	PBE	3.0775	7.21	2.08	2.17		PBE	3.0226	7.15	2.07	2.15
	HSE	3.0508	7.14	2.06	2.15		HSE	2.9945	7.07	2.04	2.14
$\text{Ti}_4\text{C}_3\text{F}_2$	Theo. ^a	3.0856	9.70	2.08	2.17	$\text{Ti}_4\text{N}_3\text{F}_2$	Theo. ^a	3.0287	9.45	2.06	2.15
	PBE	3.0844	9.67	2.07	2.17		PBE	3.0268	9.62	2.06	2.15
	HSE	3.0582	9.58	2.05	2.16		HSE	3.0041	9.49	2.04	2.14
$\text{Ti}_5\text{C}_4\text{F}_2$	Theo. ^a	3.0828	12.15	2.08	2.17	$\text{Ti}_5\text{N}_4\text{F}_2$					
	PBE	3.0794	12.19	2.08	2.17		PBE	3.0226	12.09	2.07	2.15
	HSE	3.0528	12.09	2.06	2.15		HSE	2.9947	11.96	2.04	2.13
$\text{Ti}_6\text{C}_5\text{F}_2$	PBE	3.0744	14.72	2.08	2.17	$\text{Ti}_6\text{N}_5\text{F}_2$	PBE	3.0235	14.52	2.05	2.16
	HSE	3.0456	14.63	2.06	2.15		HSE	2.9932	14.37	2.04	2.13
$\text{Ti}_7\text{C}_6\text{F}_2$	PBE	3.0719	17.24	2.08	2.17	$\text{Ti}_7\text{N}_6\text{F}_2$	PBE	3.0222	16.97	2.05	2.15
	HSE	3.0441	17.13	2.06	2.15		HSE	2.9945	16.78	2.03	2.14
$\text{Ti}_8\text{C}_7\text{F}_2$	PBE	3.0730	19.73	2.08	2.17	$\text{Ti}_8\text{N}_7\text{F}_2$	PBE	3.0194	19.45	2.05	2.15
	HSE	3.0442	19.61	2.08	2.15		HSE	2.9913	19.23	2.03	2.13
$\text{Ti}_9\text{C}_8\text{F}_2$	PBE	3.0728	22.22	2.08	2.17	$\text{Ti}_9\text{N}_8\text{F}_2$	PBE	3.0200	21.87	2.05	2.15
	HSE	3.0453	22.08	2.06	2.15		HSE	2.9932	21.62	2.03	2.13
$\text{Ti}_{10}\text{C}_9\text{F}_2$	PBE	3.0723	24.72	2.08	2.17	$\text{Ti}_{10}\text{N}_9\text{F}_2$	PBE	3.0179	24.34	2.05	2.15
	HSE	3.0448	24.56	2.06	2.15		HSE	2.9874	24.13	2.03	2.13

^a Ref. 24, VASP-PBE.

except for Ti_2NH_2 , where the HSE06 lattice parameter is 0.15 Å longer. For both carbides and nitrides, the oxygen terminated MXenes have the shortest $d_{\text{Ti-T}}$ and longest $d_{\text{Ti-X}}$ bond length, implying a strong interaction between surface Ti atoms and O termination. Alternatively, the hydroxyl terminated MXenes have the largest lattice parameters and longest $d_{\text{Ti-T}}$ bond lengths. Comparing carbides with nitrides, we find that the carbides have larger lattice constant and longer bond lengths, correlating with the atomic radii difference between carbon and nitrogen. With increasing n , taking fluorinated MXenes as an example, the lattice constant of carbides increases initially, then decreases slowly when $n > 5$. On the other hand, the lattice constant of nitrides drops rapidly at $n = 2$, then it remains the same around 3.0 Å. For MXenes covered with other functional groups, similar behaviors have been observed.

B. Magnetic and electronic properties

We checked for possible magnetic ground states of MXenes with fully relaxed spin-polarized calculations. We find that only the $\text{Ti}_{n+1}\text{X}_n$ monolayers are magnetic. The magnetization results mainly from the $3d$ electrons of surface Ti atoms. Taking Ti_2X as an example, the magnetic moments of surface Ti and topsite C/N atoms are about 0.982 and 0.065 μ_B per atom for Ti_2C and 0.619 and 0.027 μ_B per atom for Ti_2N , respectively.

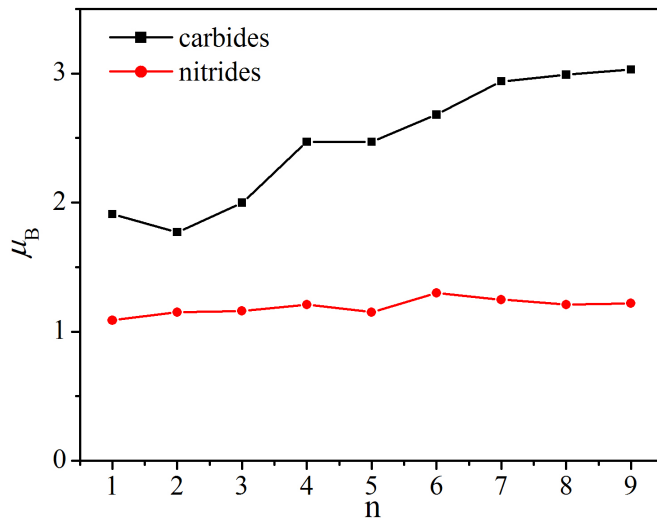


FIG. 3. (color online) Evolution of total magnetic moment of pure carbide (black line) and nitride (red line) monolayers as a function of the layer thickness. Carbides and nitrides behave differently.

The total magnetic moment of carbides and nitrides as a function of n are presented in Fig. 3. As we can see, carbides and nitrides show a different behavior. The total magnetic moment of carbides increases from 2 to 3 μ_B , while in nitrides the total magnetic moment fluctuates around 1.2 μ_B . Upon functionalization, the magnetism of MXenes disappeared.

With the appropriate ground-states, we can now move to study the electronic properties of functionalized MXenes. We first examine the electronic properties of the thinnest Ti_2XT_2 monolayers. The calculated PBE and HSE06 band structures of Ti_2XT_2 monolayers are shown and compared with pure MXenes and parent MAX phases in Fig. 4. The PBE and HSE06 functionals give the similar results, and all of these materials are metals, with the notable exception of Ti_2CO_2 . PBE functional predicts a band gap of 0.24 eV for Ti_2CO_2 , while the gap is widened to 0.88 eV by HSE06 hybrid functional. Since HSE06 is expected to be more reliable than PBE for band gaps, we predict a near 1eV band gap for this material. Unless specifically mentioned, the following results are all calculated with HSE06.

By examining the band structures near the Fermi level, we find that the Fermi energy

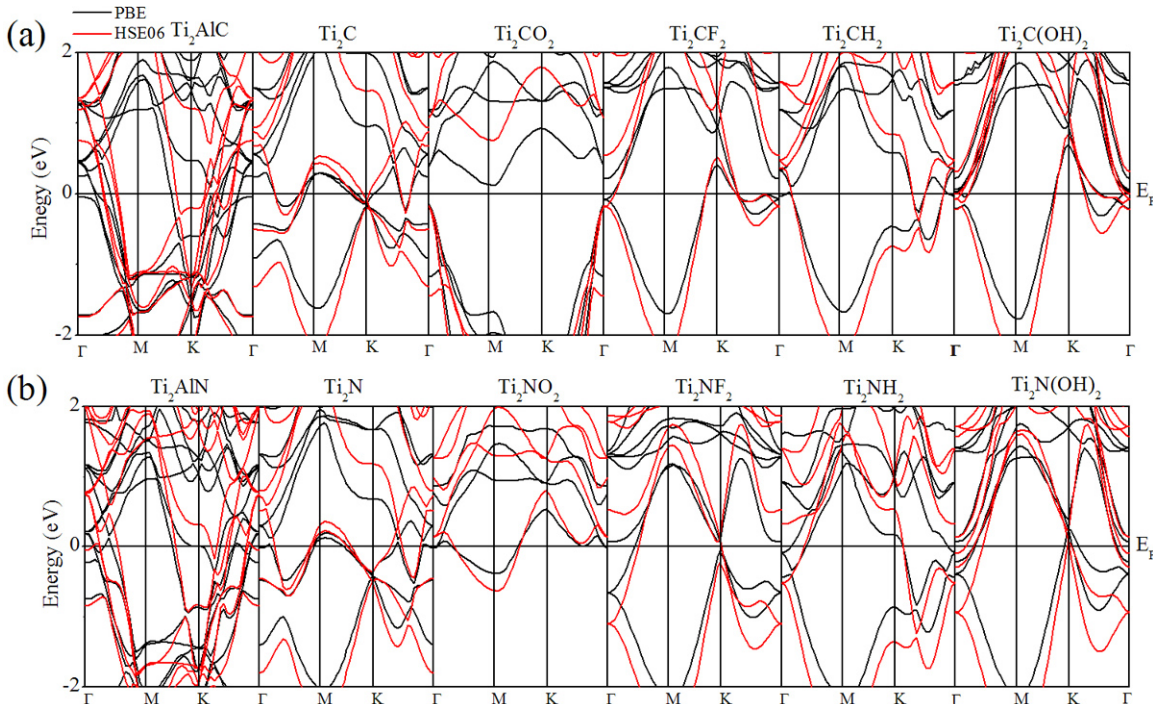


FIG. 4. (color online) (a) and (b) Band structures of Ti_2CT_2 and Ti_2NT_2 , and related MXenes and MAX phases. The HSE06 results are similar to PBE results, with modest changes to the band structures. The band-gap of Ti_2CO_2 is widened by HSE06.

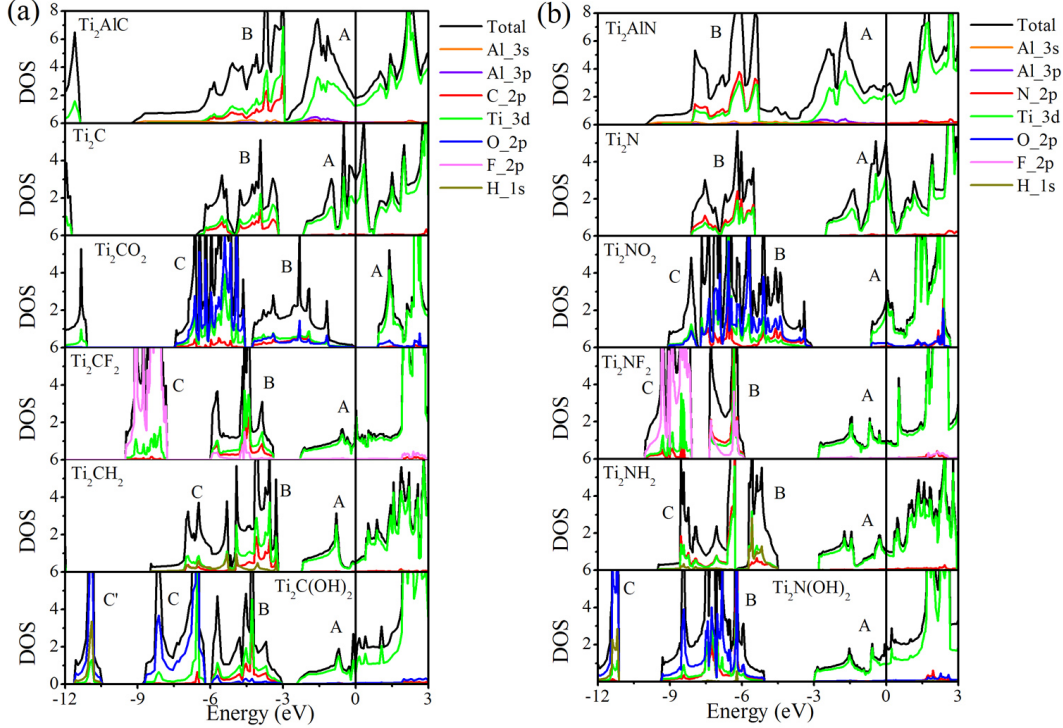


FIG. 5. (color online) (a) and (b) Partial density of states of Ti_2CT_2 and Ti_2NT_2 , and related MXenes and MAX phase computed using the HSE06 functional.

shifts down after removing Al atoms from MAX phases, and then it shifts down in energy again after the MXenes surfaces are terminated (Fig. 4). To give a better description of the electronic properties, the partial density of states (PDOS) of these materials are shown in Fig. 5. As we can see, for MAX phases, the DOS at Fermi level ($N(E_F)$) is dominated by Ti 3d orbitals. The valence states below Fermi level can be divided into two sub-bands which are formed by hybridized Ti 3d–C 2p and Ti 3d–Al 3s orbitals between -10 and -3 eV (band B), and Ti 3d–Al 3p orbitals near Fermi level (band A). These mixed states correspond to the Ti–C and Ti–Al bands. By extracting Al atoms, the bands A and B are narrowed, and a gap opens between them. The $N(E_F)$ increases from 1.88 to 3.15 and from 2.77 to 4.84 for carbides and nitrides, due to the breaking of Ti–Al bonds, respectively. After functionalization, the Fermi level shifts to lower energy states and the $N(E_F)$ decreases due to the new energy states between Ti and terminations. For carbides, band C is formed below band B corresponding to the hybridization between Ti and functional groups. Different from carbides, except for the newly formed band C, the functional groups also have a large contribution for band B in nitrides. Comparing Ti_2CO_2 with other materials, we find that

TABLE IV. Evolution of DOS at Fermi level as a function of n of functionalized MXenes computed using the HSE06 functional.

$\text{Ti}_{n+1}\text{C}_n$	O	F	H	OH	$\text{Ti}_{n+1}\text{C}_n$	O	F	H	OH
Ti_2C	0	2.156	0.566	1.916	Ti_2N	2.562	0.941	1.045	1.817
Ti_3C_2	0.575	2.026	0.823	2.876	Ti_3N_2		1.279		
Ti_4C_3	0.98	2.013	2.902	3.176	Ti_4N_3	3.895	2.601	2.313	3.881
Ti_5C_4	0.915	4.392	5.124	4.013	Ti_5N_4		4.895		
Ti_6C_5		7.284			Ti_6N_5		3.407		
Ti_7C_6	0.998	6.579	8.082	6.214	Ti_7N_6		6.501		
Ti_8C_7		5.835			Ti_8N_7		4.072		
Ti_9C_8		5.444			Ti_9N_8		7.363		
Ti_{10}C_9		5.248			Ti_{10}N_9		8.107		

band B is equally contributed by Ti $3d$, C $2p$, and O $2p$ orbitals. The strong hybridization of Ti $3d$ -C $2p$ and Ti $3d$ -O $2p$ is responsible for the semiconducting behavior of Ti_2CO_2 .

Since the $N(E_F)$ is very important for the surface chemistry of layered materials, the evolution of the value of $N(E_F)$ of functionalized MXenes as a function of n has been studied and is shown in Table IV. Firstly, we notice that starting from $n = 2$, the carbides with oxygen termination are metals. By looking at the PDOS $\text{Ti}_{n+1}\text{C}_n\text{O}_2$ (Fig. 6), it is clear that the contribution of O $2p$ orbitals to band B decreases as n increased. Starting from $n = 2$, Band B is dominated by mixed Ti $3d$ and C $2p$ bands and connected with band A, which is similar to the case observed in MAX phases. Therefore, the weaker Ti-O coupling in energy states B results in the metallic phase of $\text{Ti}_{n+1}\text{C}_n\text{O}_2$. Secondly, we find that, for carbides, the fluorine terminated MXenes have the largest DOS at Fermi level and the oxygen terminations have the lowest one, while it is opposite for nitrides. Thirdly, there is a clear trend that, for both carbides and nitrides covered with functional groups, the value of $N(E_F)$ increases with increased n . For instance, taking fluorinated MXenes as an example, $N(E_F)$ of $\text{Ti}_{n+1}\text{C}_n\text{F}_2$ is around 2 for $n \leq 3$, then it increases rapidly from 2.013 ($n = 3$) to 7.284 ($n = 5$), which is about 3.5 times higher. It decreases slowly to 5.248 ($n = 9$), which is still 2.5 times higher than the thinnest MXenes. Alternatively, $N(E_F)$ of $\text{Ti}_{n+1}\text{N}_n\text{F}_2$ continuously increases from 0.941 ($n = 1$) to 8.107 ($n = 9$), which is about 8 times higher. The similar behavior is also observed in MXenes with other functional groups. The huge difference of $N(E_F)$ between the thin ($n < 5$) and thick ($n \geq 5$) functionalized MXenes implies their surface properties should be very different and the thick layers may

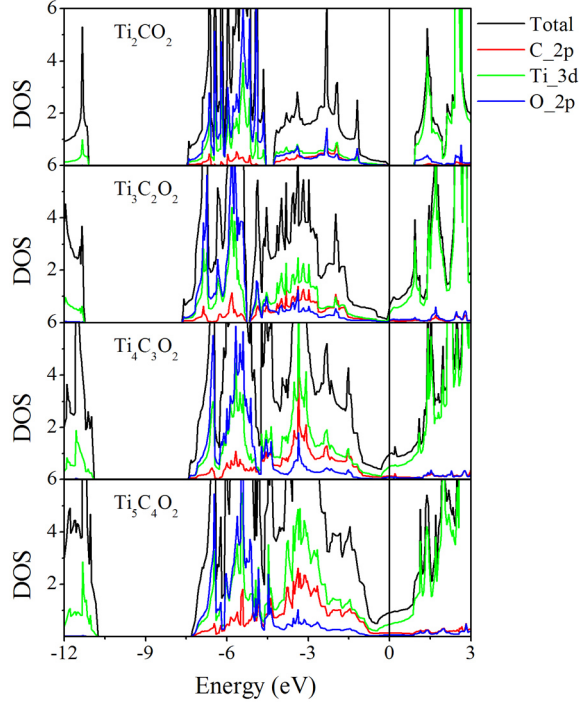


FIG. 6. (color online) Partial density of states of $\text{Ti}_{n+1}\text{C}_n\text{O}_2$ up to $n = 4$ computed using the HSE06 functional.

have higher chemical activity. The conductivity is expected to be similarly effected.

To better understand the trend, we examine the PDOS of $\text{Ti}_{n+1}\text{X}_n\text{F}_2$ as a function of n as shown in Fig. 5 and compare it with bulk titanium carbide (TiC) and nitride (TiN). One can observe that at $n = 1$, the peak of the conduction states is about 2 eV above the Fermi level for both carbide and nitride. This can also be seen from the band structures (Fig. 8). We also find that, for carbide, there are energy bands crossing the Fermi level along all the high symmetry directions of the Brillouin Zone. However, the energy bands only cross the Γ -M and K- Γ directions in nitride. This could be the reason that $N(E_F)$ of Ti_2NF_2 is about half of Ti_2CF_2 . With increasing n , the Fermi level shifts down continuously and there are more bands forming near the Fermi level (Fig. 8) related to the Ti-C coupling (Fig. 7). For carbides, we observe a sharp narrow DOS peak appears around 0.5 eV above the Fermi level at $n = 3$, corresponding to the less dispersed band along the Γ -M-K direction (Fig. 8(a)). This peak shifts down and come across the Fermi level at $n = 4$, where we start to see the increasing of $N(E_F)$. The latter reaches the maximum when Fermi level locates at the top of this peak at $n = 5$. For higher n , this band keeps shifting down and goes below

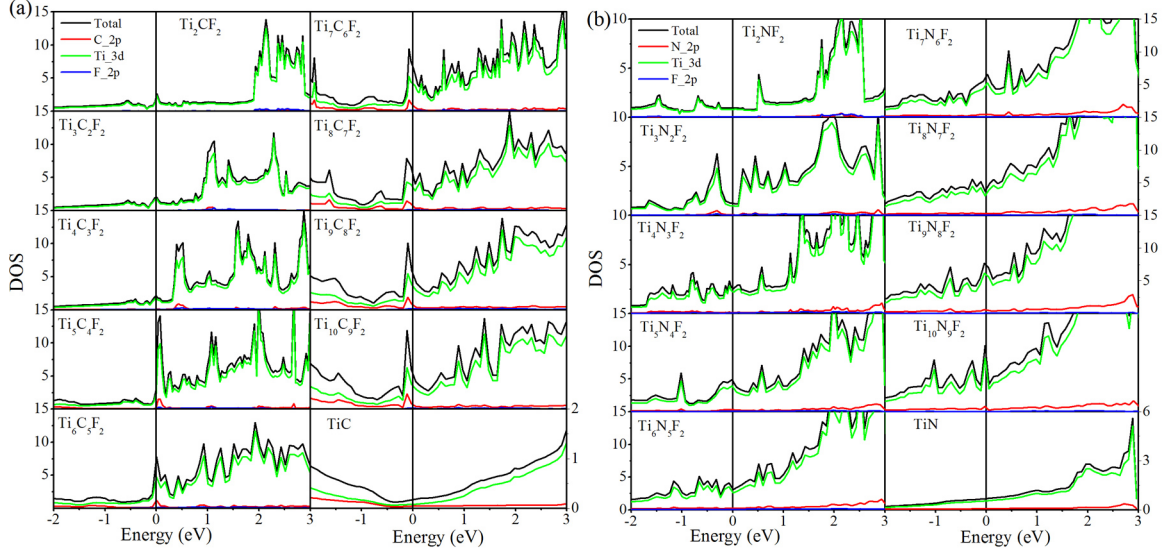


FIG. 7. (color online) (a) and (b) Partial density of states of $\text{Ti}_{n+1}\text{C}_n\text{F}_2$ and $\text{Ti}_{n+1}\text{N}_n\text{F}_2$, compared with bulk TiC and TiN phase, computed using the HSE06 functional.

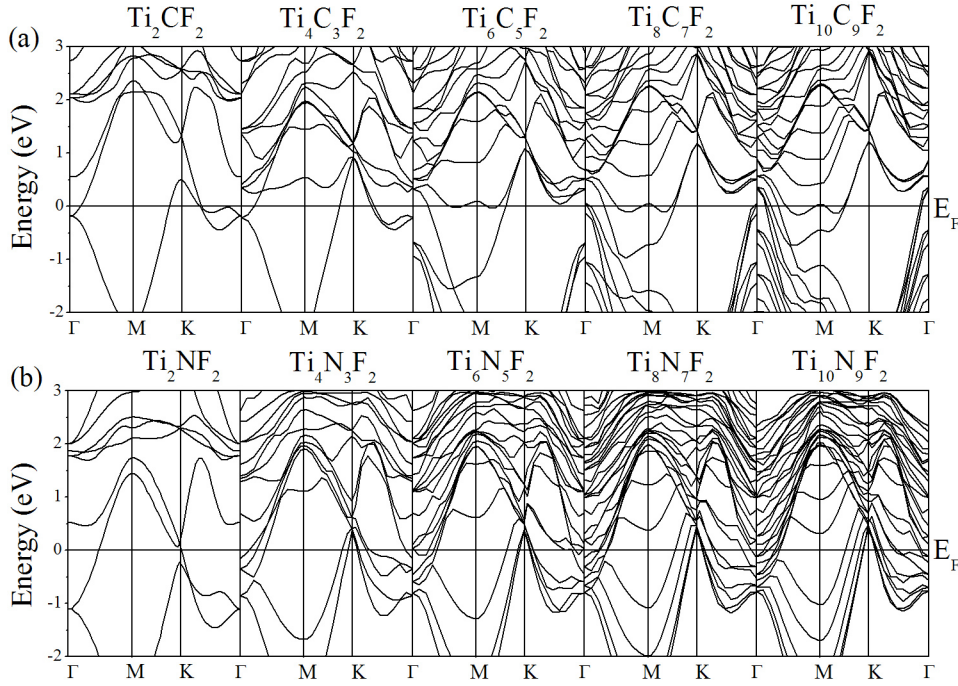


FIG. 8. (color online) (a) and (b) Band structures of $\text{Ti}_{n+1}\text{C}_n\text{F}_2$ and $\text{Ti}_{n+1}\text{N}_n\text{F}_2$ at $n = 1, 3, 5, 7,$ and 9 computed using the HSE06 functional. Clearly, there are more bands forming near the Fermi level with increased n .

the Fermi level (Fig. 8(a)). Moreover, there are fewer bands cross the Fermi level in the K- Γ direction. Although a new band is approaching the Fermi level, the value of $N(E_F)$ is still decreased. For nitrides, we don't see the sharp narrow DOS peak as well as the flat band above the Fermi level as in carbides. Due to the shifting down of the Fermi level, the bands start to cross the M-K direction at $n = 2$, and steadily increasing numbers of bands cross the Γ -M and K- Γ directions as n increases. Therefore, we observe a continuous increasing of $N(E_F)$ in nitrides. We should point out, for $n = 5$, and 7, the Fermi level is located in the bottom of a small valley, so the $N(E_F)$ decreases a little compared to other nitrides. Moreover, the DOS of carbides and nitrides show some characters as of bulk TiC and TiN when $n \geq 7$. However, the contribution of C $2p$ orbital near the Fermi level is more significant in the thicker MXenes than bulk. Thus, the thicker MXenes can still be considered as 2D materials.

V. CONCLUSION

In summary, we have systematically studied the structural and electronic properties of functionalized $Ti_{n+1}C_n$ and $Ti_{n+1}N_n$ with n up to 9, using PBE and HSE06 functionals. We show that both PBE and HSE06 predict very similar structures and electronic structures. The HSE06 functional predicts structural parameters smaller than PBE by $0.02 \sim 0.03$ Å and gives similar band structures. The functional groups are more likely to bond with Ti atoms as the electron donor. Without terminations, MXenes are magnetic, with the magnetism primarily due to surface Ti atoms. Upon functionalization, the magnetism is removed. All the functionalized MXenes are metallic except for semiconducting Ti_2CO_2 , due to the strong Ti $3d$ and O $2p$ orbital hybridization near the Fermi level. The electronic properties of thicker MXenes ($n \geq 5$) are different from the thinnest, where the $N(E_F)$ of thicker MXenes is about $3.5 \sim 8$ times higher. This indicates that the thinnest and more thick MXenes are likely to display differing properties. Our simulations shed some light on selecting proper MXene systems for possible applications and future experimental and theoretical studies are encouraged in this field.

ACKNOWLEDGMENTS

We thank Prof. Yury Gogotsi for helpful discussions and for bringing MXenes to our attention. V. Mochalin made helpful comments on the manuscript. This work was supported as part of the Fluid Interface Reactions, Structures and Transport (FIRST) Center, an Energy Frontier Research Center funded by the U.S. Department of Energy, Office of Science, Office of Basic Energy Sciences. This research used resources of the National Energy Research Scientific Computing Center, which is supported by the Office of Science of the U.S. Department of Energy under Contract No. DE-AC02-05CH11231.

* yxe@ornl.gov

- ¹ K. Novoselov, A. K. Geim, S. Morozov, D. Jiang, Y. Zhang, S. Dubonos, I. Grigorieva, and A. Firsov, *Science* **306**, 666 (2004).
- ² C. Berger, Z. Song, X. Li, X. Wu, N. Brown, C. Naud, D. Mayou, T. Li, J. Hass, A. N. Marchenkov, *et al.*, *Science* **312**, 1191 (2006).
- ³ Y. Zhang, Y.-W. Tan, H. L. Stormer, and P. Kim, *Nature* **438**, 201 (2005).
- ⁴ M. D. Stoller, S. Park, Y. Zhu, J. An, and R. S. Ruoff, *Nano Lett.* **8**, 3498 (2008).
- ⁵ Y. Yoon, K. Ganapathi, and S. Salahuddin, *Nano Lett.* **11**, 3768 (2011).
- ⁶ A. C. Neto, F. Guinea, N. Peres, K. Novoselov, and A. Geim, *Rev. Mod. Phys.* **81**, 109 (2009).
- ⁷ J. J. Yoo, K. Balakrishnan, J. Huang, V. Meunier, B. G. Sumpter, A. Srivastava, M. Conway, A. L. Mohana Reddy, J. Yu, R. Vajtai, *et al.*, *Nano Lett.* **11**, 1423 (2011).
- ⁸ H. Ramakrishna Matte, A. Gomathi, A. K. Manna, D. J. Late, R. Datta, S. K. Pati, and C. Rao, *Angew. Chem. Int. Ed.* **122**, 4153 (2010).
- ⁹ D. Pacile, J. Meyer, C. O. Girit, and A. Zettl, *Appl. Phys. Lett.* **92**, 133107 (2008).
- ¹⁰ K. Novoselov, D. Jiang, F. Schedin, T. Booth, V. Khotkevich, S. Morozov, and A. Geim, *Proc. Natl. Acad. Sci. U.S.A.* **102**, 10451 (2005).
- ¹¹ P. Eklund, M. Beckers, U. Jansson, H. Högberg, and L. Hultman, *Thin Solid Films* **518**, 1851 (2010).
- ¹² M. W. Barsoum, *Prog. Solid State Chem.* **28**, 201 (2000).
- ¹³ M. W. Barsoum and M. Radovic, *Annu. Rev. Mater. Sci.* **41**, 195 (2011).

- ¹⁴ X. Wang and Y. Zhou, *J. Mater. Sci. Technol.* **26**, 385 (2010).
- ¹⁵ Z. Sun, *Int. Mater. Rev.* **56**, 143 (2011).
- ¹⁶ M. Naguib, M. Kurtoglu, V. Presser, J. Lu, J. Niu, M. Heon, L. Hultman, Y. Gogotsi, and M. W. Barsoum, *Adv. Mater.* **23**, 4248 (2011).
- ¹⁷ M. Naguib, O. Mashtalir, J. Carle, V. Presser, J. Lu, L. Hultman, Y. Gogotsi, and M. W. Barsoum, *ACS nano* **6**, 1322 (2012).
- ¹⁸ A. Enyashin and A. Ivanovskii, *Comput. Theor. Chem.* **989**, 27 (2012).
- ¹⁹ M. Kurtoglu, M. Naguib, Y. Gogotsi, and M. W. Barsoum, *MRS Commun.* **2**, 133 (2012).
- ²⁰ J. Come, M. Naguib, P. Rozier, M. Barsoum, Y. Gogotsi, P.-L. Taberna, M. Morcrette, and P. Simon, *J. Electrochem. Soc.* **159**, A1368 (2012).
- ²¹ M. Naguib, J. Come, B. Dyatkin, V. Presser, P.-L. Taberna, P. Simon, M. W. Barsoum, and Y. Gogotsi, *Electrochem. Commun.* **16**, 61 (2012).
- ²² Q. Tang, Z. Zhou, and P. Shen, *J. Am. Chem. Soc.* **134**, 16909 (2012).
- ²³ O. Mashtalir, M. Naguib, V. N. Mochalin, Y. DallAgnese, M. Heon, M. W. Barsoum, and Y. Gogotsi, *Nat. Commun.* **4**, 1716 (2013).
- ²⁴ M. Khazaei, M. Arai, T. Sasaki, C.-Y. Chung, N. S. Venkataramanan, M. Estili, Y. Sakka, and Y. Kawazoe, *Adv. Funct. Mater.* **23**, 2185 (2013).
- ²⁵ I. Shein and A. Ivanovskii, *Comput. Mater. Sci.* **65**, 104 (2012).
- ²⁶ N. J. Lane, M. W. Barsoum, and J. M. Rondinelli, *EPL* **101**, 57004 (2013).
- ²⁷ G. Kresse and J. Furthmüller, *Phys. Rev. B* **54**, 11169 (1996).
- ²⁸ P. E. Blöchl, *Phys. Rev. B* **50**, 17953 (1994).
- ²⁹ J. P. Perdew, K. Burke, and M. Ernzerhof, *Phys. Rev. Lett.* **77**, 3865 (1996).
- ³⁰ J. Heyd, G. E. Scuseria, and M. Ernzerhof, *J. Chem. Phys.* **118**, 8207 (2003).
- ³¹ J. Paier, M. Marsman, K. Hummer, G. Kresse, I. C. Gerber, and J. G. Ángyán, *J. Chem. Phys.* **124**, 154709 (2006).
- ³² J. Heyd, G. E. Scuseria, and M. Ernzerhof, *J. Chem. Phys.* **124**, 219906 (2006).
- ³³ V. Eyert, *Phys. Rev. Lett.* **107**, 016401 (2011).
- ³⁴ B. Manoun, F. Zhang, S. Saxena, T. El-Raghy, and M. Barsoum, *J. Phys. Chem. Solids* **67**, 2091 (2006).
- ³⁵ H. Högberg, P. Eklund, J. Emmerlich, J. Birch, and L. Hultman, *J. Mater. Res.* **20**, 779 (2005).
- ³⁶ L. Zheng, J. Wang, X. Lu, F. Li, J. Wang, and Y. Zhou, *J. Am. Ceram. Soc.* **93**, 3068 (2010).

- ³⁷ J. Zhang, B. Liu, J. Wang, and Y. Zhou, *J. Mater. Res.* **24**, 39 (2009).
- ³⁸ M. Barsoum, C. Rawn, T. El-Raghy, A. Procopio, W. Porter, H. Wang, and C. Hubbard, *J. Appl. Phys.* **87**, 8407 (2000).
- ³⁹ C. Li and Z. Wang, *J. Appl. Phys.* **107**, 123511 (2010).
- ⁴⁰ V. Keast, S. Harris, and D. Smith, *Phys. Rev. B* **80**, 214113 (2009).
- ⁴¹ Z. Hou, X. Wang, T. Ikeda, S.-F. Huang, K. Terakura, M. Boero, M. Oshima, M.-a. Kakimoto, and S. Miyata, *J. Phys. Chem. C* **115**, 5392 (2011).